EPJ manuscript No.
(will be inserted by the editor)

arXiv:cond-mat/0504414v1 [cond-mat.soft] 18 Apr 2005

Non-linear Osmotic Brush Regime: Simulations and mean-field theory *

Ali Naji[1,2,a], Roland R. Netz[1,2,b], and Christian Seidel[2,c]

[1] Physics Department, Technical University of Munich, D-85748 Garching, Germany.
[2] Max-Planck Institute of Colloids and Interfaces, Am Mühlenberg, D-14476 Golm, Germany.

Received: date / Revised version: date

Abstract. We investigate polyelectrolyte brushes in the osmotic regime using both theoretical analysis and molecular dynamics simulation techniques. In the simulations at moderate Bjerrum length, we observe that the brush height varies weakly with grafting density, in contrast to the accepted scaling law, which predicts a brush thickness independent of the grafting density. We show that such behavior can be explained by considering lateral electrostatic effects (within the non-linear Poisson-Boltzmann theory) combined with the coupling between lateral and longitudinal degrees of freedom due to the conserved polymer volume (which are neglected in scaling arguments). We also take the non-linear elasticity of polyelectrolyte chains into consideration, which makes significant effects as chains are almost fully stretched in the osmotic regime. It is shown that all these factors lead to a non-monotonic behavior for the brush height as a function of the grafting density. At large grafting densities, the brush height increases with increasing the grafting density due to the volume constraint. At small grafting densities, we obtain a re-stretching of the chains for decreasing grafting density, which is caused by lateral electrostatic contributions and the counterion-condensation process at polyelectrolyte chains. These results are obtained assuming all counterions to be trapped within the brush, which is valid for sufficiently long chains of large charge fraction.

PACS. 61.25.Hq Macromolecular and polymer solutions; polymer melts; swelling – 36.20.-r Macromolecules and polymer molecules – 61.20.Qg Structure of associated liquids: electrolytes, molten salts, etc.

1 Introduction

In recent years, polyelectrolyte brushes have been subject of extensive investigations both theoretically [1,2,3,4,5,6,7,8,9,10,11,12,13,14,15,16] and experimentally [17,18,19,20,21,22,23,24,25,26,27]. Polyelectrolyte brushes are layers of charged polymer chains densely end-grafted onto surfaces of various geometries. They have important technological applications notably in stabilization of colloidal dispersions in polar media, where forces between colloidal particles (coated by grafted polyelectrolytes) are modified and may be controlled in order to prevent flocculation [28,29]. Recent investigations [1,2,3,4,5,6,7,8,9,10,11,12,13,14,15,16,17,18,19,20,21,22,23,24,25,26,27] have revealed the detailed phase behavior of charged brushes over a wide range of system parameters, namely, grafting density and charge fraction of chains. (Here we consider only planar brushes with no added salt.) It is known from scaling theories as well as from self-consistent field studies that the interplay between steric, entropic and electrostatic contributions results in a variety of different scaling relations for the equilibrium height of the brush.

In strongly charged brushes with a large effective charge density of grafted polyelectrolytes, *i.e.* when both grafting density and charge fraction of polyelectrolyte chains are sufficiently large, effectively all of the counterions are trapped inside the brush. Over a certain range of charge fractions and grafting densities, the repulsive osmotic pressure of counterions is the major effect that tends to swell the chains and balances their elastic stretching pressure. This regime is known as the osmotic brush regime, where the equilibrium thickness of the brush was obtained by scaling arguments to be independent of the grafting density [3,4]. The osmotic brush height may, however, exhibit a weak dependence on the grafting density as a result of non-uniform counterion distribution inside the brush. Specifically, variation of the counterion density profile in the direction normal to the anchoring plane (which may be caused by partial diffusion of counterions outside the brush layer) leads to a logarithmic dependence on the grafting density [11]. A weak dependence of the brush height on grafting density may also be produced by lateral inhomogeneities as will be addressed in this paper.

---

[*] A revised version of Ref. [34] with corrections in the simulation part from C. Seidel, Macromolecules **38**, 2540 (2005).

[a] e-mail: `naji@ph.tum.de`

[b] e-mail: `netz@ph.tum.de`

[c] e-mail: `seidel@mpikg-golm.mpg.de`

The crossover between these two mechanisms is regulated by the chain charge fraction and grafting density. In the regime of large grafting densities, steric effects dominate over electrostatic interactions and the excluded-volume repulsion (in good solvent conditions) balances the elastic pressure, leading to the so-called quasi-neutral brush regime [4,9]. The effects of excluded-volume interactions have also been studied in poor solvent conditions [5]. On the other hand, for larger charge fractions, the electrostatic correlations due to Debye-Hückel interactions between mobile counterions and oppositely charged monomers may produce a dominant attractive pressure balancing the excluded-volume repulsion [4,13]. This leads to a collapsed brush regime, which has also been obtained in previous molecular dynamics simulations [13,14,15].

In weakly charged brushes (which are not considered in this paper), the counterion cloud extends far beyond the brush height and the osmotic pressure of the counterions becomes irrelevant against uncompensated electrostatic repulsion between charged monomers. This results in the charged or Pincus brush regime, where the elastic and the electrostatic pressures are balanced [3]. Details of the phase diagram and transitions between these regimes have been discussed extensively in the literature [1,2,3,4,5,6,7,8,9,10,11,12,13].

In recent molecular dynamics simulations [16], structure and equilibrium properties of salt-free planar osmotic brushes have been studied at moderate Bjerrum length. For moderate values of charge fraction and grafting density, it has been observed that the counterions are mostly confined within the brush and generate an almost step-like density profile in the direction normal to the anchoring plane. In contrast, counterions exhibit a non-uniform distribution in lateral directions. In this situation, the simulated brush thickness varies weakly with the grafting density in contrast to the standard scaling law [3,4].

In scaling studies, it is commonly assumed that the counterions are distributed uniformly in lateral directions parallel to the anchoring plane and that the elasticity of chains is obtained from a linear (Gaussian) model. In this paper, we present a mean-field model for the osmotic brush, in which we consider corrections to both of these assumptions: Firstly, we take into account *lateral* electrostatic effects including lateral variation of the counterion density profile around polyelectrolyte chains within the framework of the non-linear Poisson-Boltzmann (PB) theory, and secondly, we use a freely-jointed-chain model to mimic non-linear elastic stretching of the polyelectrolyte chains. Moreover, we take into account excluded-volume interactions between particles as well as the conserved polymer volume as the chain dimensions change, as will be described below. The results of our model for the behavior of the brush thickness, which we refer to as the *non-linear osmotic brush regime*, display a non-monotonic dependence on the grafting density. In particular, at moderate grafting densities, we find that the brush height weakly increases with the grafting density arising as a result of the interplay between lateral electrostatics and the coupling effects. This behavior will be compared with simulation results displaying a reasonable agreement. A weak dependence of the brush height on grafting density has also been observed in recent experiments [26,27] and has been compared with the non-linear osmotic brush predictions obtained using simple scaling arguments [26]. At small grafting densities, our model predicts re-stretching of the chains by lowering the grafting density, which is caused by an increasing electrostatic pressure acting on the chains in this limit. As we shall demonstrate, this behavior is regulated by the counterion-condensation process around the chains, which is captured within the non-linear PB theory. This regime has not been investigated in simulations and experiments yet, and we propose that one needs long chains to obtain this behavior (see the Discussion).

An inhomogeneous distribution of counterions in lateral directions has been recently observed both in simulation [14,15,16] and experiment [20,22,24,25]. Analyzing experimental data on spherical charged brushes, Muller *et al.* [22] observe that the counterion distribution around polyelectrolyte chains indeed follows the the non-linear PB predictions as obtained within the cylindrical-cell-model approach [30,31]. Other experiments indicate that a large fraction of counterions binds strongly to the polyelectrolyte chains, thus counterions are not evenly distributed inside the brush [20,24,25]. On the other hand, the non-linear elasticity, which accounts for the finite extensibility of the chains, appears to be essential for strongly charged brushes at moderate grafting densities, as polyelectrolyte chains in these situations are found to be stretched up to 60-80% of their contour length [16,18,19,20,22,24,26,27]. Non-linear elasticity models have also been used in previous works [10] (but without considering lateral effects as done here). It is important to note that the non-linear elasticity by itself can not generate a grafting-density dependence for the brush height [12].

We shall neglect the variation of the counterionic density profile in the direction normal to the anchoring plane and assume that all counterions are trapped within the brush. In the range of parameters, where a sizable fraction of counterions could leave the brush layer, the step form of the density profile in the normal direction is changed and may be calculated using self-consistent field (SCF) techniques [1,2,6,8,10,11]. The SCF study of Zhulina and Borisov [11] indeed shows that at large grafting densities (osmotic regime), the variation of the density profile in the normal direction gives rise to a logarithmic dependence of the brush height on the grafting density. Such a dependence is obtained by treating the electrostatic effects at the non-linear level using the PB equation but assuming that the concentration of counterions (and that of monomers) is smeared in lateral directions [11]. Our model, therefore, describes the complementary limit, which can be achieved by taking sufficiently long chains of large charge fraction (even at low grafting densities) as will be examined later.

In the present study, we account for the volume interaction between counterions and polyelectrolyte chains using a closest-approach distance, but neglect the excluded-volume interactions between counterions themselves, which may be justified in the considered range of parameters. In addition, the effective volume of the polyelectrolyte chain, which is not accessible for counterions, is assumed to be constant: when chains shrink (at a fixed grafting density), the available volume for counterions decreases leading to an increasing osmotic pressure. Such a coupling between longitudinal and lateral degrees of freedom is a very simple way to mimic the back influence of the conformational changes of the chains on the true volume available for counterions inside the brush and their osmotic pressure.

2 The geometry of the model

The model which shall be employed in the present study to calculate the electrostatic free energy of the brush is based on the commonly-used cell model for rod-like polyelectrolyte solutions [32,33]. Each polyelectrolyte chain in the brush is assumed to have N spherical monomers of the same *diameter* b_0 among which a fraction of f is charged with a charge valency of q. We assume that each single chain is symmetrically enclosed in a cylindrical unit cell with radius D, which is determined by the grafting density ρ_{a}. The chains length, L, is assumed to be much larger than the radius of the cell, $L \gg D$. Furthermore, each polyelectrolyte chain is modeled as a cylindrical rod (which we may refer to as the polyelectrolyte rod) with the same length and some radius $R \leq D$. We suppose that the total volume of the rod is constant, *i.e.*, $R^2 L = R_0^2 L_0$, where L_0 and R_0 stand for the length and radius associated with its fully stretched conformation; L_0 is taken equal to the contour length of the chain, $L_0 = N b_0$, but R_0 can be generally different from the radius of the monomers due to different possibilities to choose a cylindrical rod model for a polyelectrolyte chain [34]. We restrict our discussion to a model in which $R_0 = b_0/2$ (Figure 1a).

The electric charge of the polyelectrolyte chain, qfN, is assumed to be uniformly distributed over the surface of the rod with a linear charge density of τ (all in units of elementary charge e). There is a fixed number of oppositely charged counterions, N_c, with charge valency of q_c and radius of r_c confined inside each unit cell, such that the electroneutrality condition, $\tau L = qfN = q_c N_c$, is fulfilled. (The charge valencies q and q_c, and also τ, are defined to be positive.) Solvent is treated as a continuum background characterized completely by its dielectric constant ε, and no additional salt is present in the system.

In the simulation model, grafting points form a square lattice with the lattice spacing of $2D_{sim}$ and thus, a grafting density of $\rho_{\mathrm{a}} = 1/(4D_{sim}^2)$. A natural space-filling choice of unit cell for this system is a square unit cell with the edge size of $2D_{sim}$. Since the analytical solution for the counterion distribution is only available for a cylindrical unit cell, we have to map the square simulation box to a cylindrical box. (Note that experimentally, the grafting-point distribution is highly irregular and thus different from both simulation and analytical model.) There are different ways to adopt a cylindrical unit cell for such a planar brush as discussed in detail in Ref. [34]. Here we choose a cylindrical cell with the diameter, $2D$, equal to the lattice spacing of the square lattice as shown in Figure 1b, where $D = D_{sim}$.

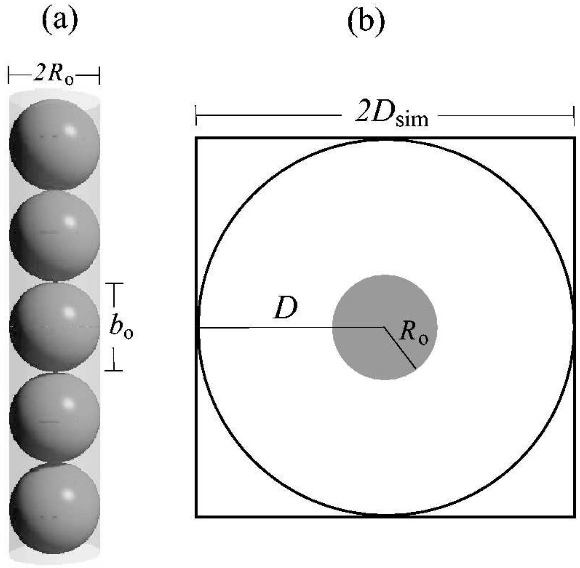

Fig. 1. The model used for the polyelectrolyte chain (a) and the cylindrical unit cell (b) for the brush as discussed in the text. The unit cell boundary in the simulations is shown by a square.

3 Non-linear osmotic brush regime within mean-field approximation

3.1 The electrostatic free energy

The so-called mean-field or Poisson-Boltzmann theory of a cylindrical cell model for polyelectrolyte solutions has been presented long time ago [30,31,35]. In the mean-field approximation, the electrostatic correlations between neighboring cells are entirely neglected and the study of the system is therefore reduced to a single-cell study. In addition to this, correlations between counterions present in the same cell are systematically neglected, however, they remain still correlated with the polyelectrolyte rod. The system is then studied in its "ground state", where all the fluctuations are neglected as well. Then, by virtue of the electroneutrality condition, it follows that the electric field vanishes over the cell boundary.

A canonical field theory may be written for the system and the Poisson-Boltzmann (PB) theory is subsequently obtained as a saddle-point approximation to the corresponding action [36]. The canonical PB free energy per unit cell is calculated and can be written (in units of k_BT) as

$$\mathcal{F}_{N_c}^{PB} = -\frac{1}{4\pi \ell_B q_c^2}\int d\mathbf{r}\,[\frac{1}{2}(\nabla\psi)^2 + \frac{2\xi}{R}\delta(r-R)\psi(\mathbf{r})] \\ - N_c \ln[\int d\mathbf{r}\, \Omega(\mathbf{r}) e^{-\psi(\mathbf{r})}] + \mathcal{C}, \qquad (1)$$

where $\ell_B = e^2/(4\pi\varepsilon\varepsilon_0 k_B T)$ is the Bjerrum length (associated with a medium with dielectric constant of ε), $\xi = \ell_B q_c \tau$ is the Manning parameter, and $\mathcal{C}$ is a constant, which contains contributions due to self-energies, kinetic energy of counterions and other numerical constants. The geometry function $\Omega(\mathbf{r})$ takes into account the presence of hard walls and restricts the positions of mobile counterions to the cylindrical region of $R \leq r \leq D$, that is $\Omega(\mathbf{r}) = 1$ for $R \leq r \leq D$ and zero otherwise, where r denotes the radial distance from the axis of the cylindrical unit cell. As a result of the saddle-point approximation, $\delta\mathcal{F}^{PB}_{N_c}/\delta\psi = 0$, the dimensionless potential field $\psi(\mathbf{r})$ is obtained to fulfill the so-called Poisson-Boltzmann (PB) equation

$$\nabla^2\psi = \frac{2\xi}{R}\delta(r-R) - \kappa^2\Omega(\mathbf{r})e^{-\psi(\mathbf{r})}, \tag{2}$$

where $\kappa^2 = 4\pi\ell_B q_c^2 N_c/\int d\mathbf{r}\,\Omega(\mathbf{r})\exp(-\psi)$ is an unspecified factor the value of which will be fixed once we specify the reference point of the potential [37]. To calculate the electrostatic free energy, one needs to solve Eq. (2) for the potential field ψ. (Here the physical electrostatic potential reads $k_B T\psi/q_c e$.) Assuming that the polyelectrolyte rod is sufficiently long and that the solution for the potential field also has cylindrical symmetry, it follows that

$$\left(r\frac{d\psi}{dr}\right)_{r=R} = 2\xi \quad \text{and} \quad \left(r\frac{d\psi}{dr}\right)_{r=D} = 0, \tag{3}$$

where we have used the global electroneutrality condition

$$\xi L = N_c \ell_B q_c^2. \tag{4}$$

It is easily observed that the only non-trivial contribution to the PB free energy comes from the potential field in the interior region $R \leq r \leq D$, where the solution to Eqs. (2) and (3) is available due to early works by Alfrey *et al.* [30] and Fuoss *et al.* [31]. It was shown that the solution for $\psi(r)$ takes different functional forms depending on whether ξ lies below or above a threshold value ξ_c. For a polyelectrolyte rod with *fixed radius*, R, the threshold is simply given by

$$\xi_c = \frac{\ln(D/R)}{1+\ln(D/R)}, \tag{5}$$

while in our model with constant volume constraint, as we shall see later, ξ_c has to be determined from a transcendental equation.

For $\xi \leq \xi_c$, the solution reads

$$\psi(r) = \ln\left[\frac{\kappa^2 r^2}{2\beta^2}\sinh^2\left(\beta\ln\frac{r}{D} - \tanh^{-1}\beta\right)\right], \tag{6}$$

where β is given by the transcendental equation

$$\xi = \frac{1-\beta^2}{1-\beta\coth(-\beta\ln\frac{D}{R})}. \tag{7}$$

Inserting the solution Eq. (6) into the expression (1), we obtain the electrostatic free energy per number of monomers (up to an additive constant and in units of $k_B T$) as

$$\frac{\mathcal{F}^{PB}}{N} = \frac{qf}{q_c}\{-\frac{1}{\xi}[(1+\beta^2)\ln\frac{D}{R} + \ln\left(\frac{(\xi-1)^2-\beta^2}{1-\beta^2}\right) + \xi] + \ln[(\xi-1)^2-\beta^2] - \ln(2\pi\ell_B f q_c q N R^2)\}. \tag{8}$$

For $\xi \geq \xi_c$, the solution to the PB equation is

$$\psi(r) = \ln\left[\frac{\kappa^2 r^2}{2\beta^2}\sin^2\left(\beta\ln\frac{r}{D} - \tan^{-1}\beta\right)\right], \tag{9}$$

where β now satisfies the following equation

$$\xi = \frac{1+\beta^2}{1-\beta\cot(-\beta\ln\frac{D}{R})}. \tag{10}$$

Similarly, we can calculate the electrostatic free energy of the system,

$$\frac{\mathcal{F}^{PB}}{N} = \frac{qf}{q_c}\{-\frac{1}{\xi}[(1-\beta^2)\ln\frac{D}{R} + \ln\left(\frac{(\xi-1)^2+\beta^2}{1+\beta^2}\right) + \xi] + \ln[(\xi-1)^2+\beta^2] - \ln(2\pi\ell_B f q_c q N R^2)\}. \tag{11}$$

The free energies (8) and (11) have also been derived by Lifson and Katchalsky [35] using a charging process.

We note that here R represents the actual radius of the polyelectrolyte rod and thus in our model is related to the Manning parameter of the system ξ through

$$R(\xi) = R_0\sqrt{\xi/\xi_0}. \tag{12}$$

This dependence is induced by the volume constraint $R^2 L = R_0^2 L_0$, and the fact that the total charge of the rod is conserved, that means

$$\xi L = \xi_0 L_0, \tag{13}$$

where

$$\xi_0 = q_c q f\frac{\ell_B}{b_0} \tag{14}$$

is the Manning parameter associated with the fully stretched conformation of the rod. In the above formulation, counterions have been taken as point-like particles. To account for the finite size of counterions, we may define a closest approach distance between the rod and counterions, R_{ca}, to be used instead of R in the preceding equations. Assuming that the counterions have radius of r_c and recalling the actual radius of the rod R from Eq. (12), we have

$$R_{ca}(\xi) = r_c + R_0\sqrt{\xi/\xi_0}. \tag{15}$$

Note that ξ is limited from above and below due to the geometrical constraints $R_{ca} \leq D$ and $L \leq L_0$ respectively. As a result, one observes that

$$\xi_0 \leq \xi \leq \xi_u, \tag{16}$$

where

$$\xi_u = \xi_0(D-r_c)^2/R_0^2. \tag{17}$$

Finally, we remark that here the threshold Manning parameter, ξ_c, at which the functional form of the solution to the PB equation is changed, is determined from

$$\xi_c = \frac{\ln D/R_{ca}(\xi_c)}{1+\ln D/R_{ca}(\xi_c)}, \tag{18}$$

in which $R_{ca}(\xi_c)$ is given by Eq. (15). Equation (18) is in fact obtained as an extension of Eq. (5) to the present model with constant volume constraint [38].

3.2 The chain elastic free energy

We assume a freely-jointed-chain (FJC) model to calculate elastic contributions to the total free energy of polyelectrolyte chains in the brush. The exact free energy of such a chain model has a purely entropic origin and is obtained (in units of k_BT) as

$$\frac{\mathcal{F}^{FJC}}{N} = -\ln\frac{\sinh y}{y} + y\coth y - 1, \tag{19}$$

where N is the number of monomers and y is found from

$$\frac{L}{L_0} = \coth y - \frac{1}{y}, \tag{20}$$

in which L and $L_0 = Nb_0$ are end-to-end distance and contour length of the chain respectively (see Appendix A). In terms of the modeled polyelectrolyte rod, L stands for the actual height of the rod and L_0 for its height in the fully stretched situation. In the weak-stretching limit, Eqs. (19) and (20) lead to the free energy of a Gaussian chain

$$\frac{\mathcal{F}^{FJC}}{N} \approx \frac{3L^2}{2(Nb_0)^2}. \tag{21}$$

Whereas in the opposite limit of strong stretching, the model produces a non-linear elasticity with

$$\frac{\mathcal{F}^{FJC}}{N} \approx -\ln(1-\frac{L}{Nb_0}) + const., \tag{22}$$

which is dominated by the finite length of the chain. It is clear that for almost-fully-stretched chains, deviations from the Gaussian behavior will be important [10].

3.3 Optimal brush height and its limiting behavior

The total free energy of the brush per unit cell is the sum of the electrostatic and elastic free energies obtained in Eqs. (8) or (11) and (19),

$$\mathcal{F}^{tot} = \mathcal{F}^{PB} + \mathcal{F}^{FJC}. \tag{23}$$

The total free energy can be viewed as a function of the effective Manning parameter of the system, ξ, which varies according to the brush height L (see Eq. (13)). It also depends on the system parameters, namely, charge fraction of the rod, f, valency of charged monomers, q, and that of counterions, q_c, and finally on the ratio of the Bjerrum length, ℓ_B, the cell radius, D, and the counterion size, $2r_c$, to the monomer size b_0.

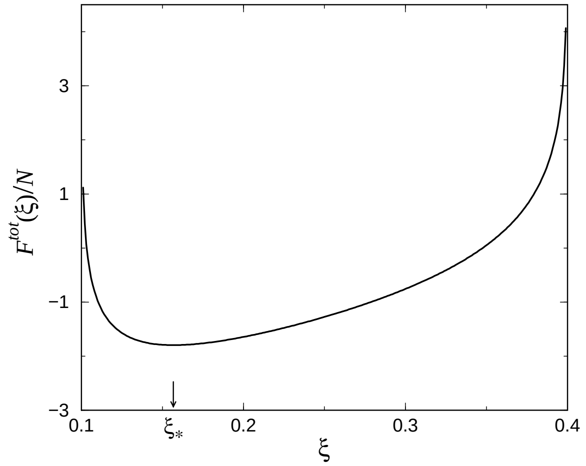

Fig. 2. Typical free energy of the present model (per number of monomers) is plotted as a function of the Manning parameter associated with the polyelectrolyte rod. Here it is calculated for $f = 1$, $\ell_B = 0.1b_0$, $q_c = q = 1$, $r_c = b_0/2$, and $D = 1.5b_0$. In this case, the lower and upper bounds for ξ are $\xi_0 = 0.1$ and $\xi_u = 0.4$ respectively. The arrow shows the location of the optimal Manning parameter $\xi_* \approx 0.16$.

The typical form of the total free energy (per unit cell) as a function of ξ is shown in Figure 2, where the free energy is calculated for $f = 1$, $\ell_B = 0.1b_0$, $q_c = q = 1$, $r_c = b_0/2$, and $D = 1.5b_0$. As explained in Section 3.1, the effective Manning parameter, ξ, is bounded from below by ξ_0, and from above by ξ_u given by Eq. (17). In this example, the lower and upper bounds on ξ are respectively $\xi_0 = 0.1$ and $\xi_u = 0.4$. As seen in the graph, the total free energy has a minimum at an intermediate value of ξ. The reason is that by decreasing ξ down to ξ_0, the chain becomes highly stretched and its elastic free energy (see Eq. (22)) and consequently its total free energy increases and eventually diverges due to its finite extensibility. In the other limit of large ξ, the available space for counterions decreases as $\xi \to \xi_u$ (equivalently $R_{ca} \to D$); thus the translational entropy of counterions dramatically decreases leading to an increasing free energy in this limit. The optimal Manning parameter, ξ_*, that minimizes the total free energy, lies somewhere between these two limits and corresponds to an optimal brush height $L_* = \xi_0 L_0/\xi_*$.

We thus obtain the optimal brush height, L_*, by minimizing the total free energy of the system (23) for various grafting densities. The results will be compared with the simulation data in Section 4. In this Section, we focus on the generic predictions of the present model for the brush height and its limiting behavior. To this end and for the sake of simplicity, we consider a simpler version of the model, in which the counterions are taken as point-like particles ($r_c = 0$). Hence, as in Eq. (12),

$$R = R_{ca} = R_0\sqrt{\xi/\xi_0}. \tag{24}$$

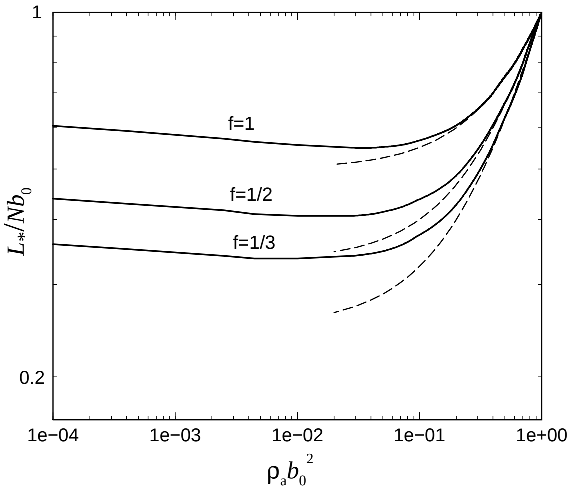

Fig. 3. Log-log plot of the rescaled optimal height of the brush as a function of the grafting density for $\ell_B = 0.1b_0$, $q_c = q = 1$ and point-like counterions (solid curves). Each of the curves corresponds to a charge fraction indicated on the graph. Dashed lines are the asymptotic behaviors obeying Eq. (28) for large grafting densities.

We also take the charge valencies as $q_c = q = 1$.

Figure 3 shows the optimal brush height plotted as a function of grafting density for the Bjerrum length of $\ell_B = 0.1b_0$, and for three different values of charge fraction $f = 1$, 1/2 and 1/3 (solid curves). It is observed that the brush height has a non-monotonic behavior as a function of grafting density: both in the limit of large grafting densities and small grafting densities, the brush height increases and eventually tends to its maximum value $L_0 = Nb_0$. Therefore, a lower bound is predicted for the equilibrium height of the brush that clearly depends on the charge fraction and the Bjerrum length. For charge fractions of $f > 1/2$ and $\ell_B/b_0 \sim 0.1$, this lower bound is about 50% of the contour length. This means that the polyelectrolyte rod remains increasingly stretched over a wide range of grafting densities. The limiting behavior of the brush height with grafting density can be understood both by asymptotic expansion of the free energy (see Appendix B) and by simple physical arguments as we present now.

First, we consider the limit of large grafting densities $\rho_a \to \rho_a^{max}$, in which $\rho_a^{max} = 1/b_0^2$ is the maximum grafting density. This corresponds to the limit of small cell radius, *i.e.* $D/R_0 \to 1$, where $R_0 = b_0/2$ in our discussion. In this limit, the available space for counterions inside the unit cell tends to zero and their entropy divergently decreases. The produced osmotic pressure becomes the major repulsive pressure swelling the rod against stretching pressure of the elasticity, and bare electrostatic effects become negligible. The entropy of counterions is then well-approximated by the entropy of an ideal gas of particles, and can be written (per number of monomers and up to an additive constant) as

$$s_{ci} \approx f \ln[\pi(D^2 - R^2)L], \tag{25}$$

where R is defined in Eq. (24) (see Appendix B). In this limit, the chain has a large extension and its elastic free energy per number of monomers is given by Eq. (22),

$$f_{elas} \approx -\ln(1 - L/L_0). \tag{26}$$

Balancing the longitudinal pressures due to these two opposing contributions,

$$\frac{\partial}{\partial L}(f_{elas} - s_{ci}) = 0 \tag{27}$$

at fixed cell radius D, we find

$$\frac{L_*(\rho_a)}{L_0} \approx \frac{f + \rho_a b_0^2}{1 + f}, \tag{28}$$

for $\rho_a b_0^2 \to 1$, where, by the definition of the model in Section 2,

$$\rho_a b_0^2 = \frac{R_0^2}{D^2}. \tag{29}$$

The expression given by Eq. (28) is plotted in in Figure 3 for the charge fractions $f = 1$, 1/2, 1/3 (dashed curves), where the coincidence with the predictions from minimizing the full free energy in Eq. (23) (solid curves) is seen at large grafting densities.

Note that within our model, the constant volume constraint dominates when $\rho_a b_0^2 \to 1$, and the linear dependence on the grafting density in Eq. (28) is induced by this constraint. It is important to note that the limiting behavior, Eq. (28), identifies the behavior of the brush height if counterions around chains are taken as a *uniform* ideal gas of particles with *no* lateral electrostatic effects (see Appendix B). But, as clearly seen from Figure 3, at lower grafting densities (*e.g.* at about $\rho_a b_0^2 \sim 0.1$, which approximately corresponds to the simulated regime–see Figures 7 and 8 below), the predicted brush height (solid curves) deviates from the above limiting line (dashed curves) displaying a weaker dependence on the grafting density. This behavior at moderate grafting densities is induced by lateral electrostatic effects, which become increasingly important and generate a minimum at intermediate grafting densities (Figure 3).

In the limit of small grafting densities $\rho_a b_0^2 \ll 1$, or equivalently $D/R_0 \gg 1$, the present model is applicable for very long chains, since only in this case, counterions will be confined within the brush. In fact, to retain counterions inside the polyelectrolyte layer, one needs to consider chains of large charge fraction with the number of monomers $N > (\rho_a b_0^2)^{-1/2}$ (see the Discussion).

In this limit, the brush height shows different asymptotic behavior in terms of the grafting density depending on whether the optimal Manning parameter, ξ_*, is below or above the threshold value ξ_c as defined in Eq. (18). Thus, we shall distinguish two different scenarios. First we look at the case when the optimal Manning parameter of the rod is smaller than the threshold Manning parameter $\xi_* < \xi_c$. For our choice of parameters in Figure 3 ($\ell_B = 0.1b_0, q = q_c = 1$), this holds for $\rho_a b_0^2 < 0.1$, as can be checked from Eq. (18). In such conditions, the counterion cloud is highly diluted (counterions effectively de-condense [39,40,41]) and there will be no electrostatic screening on the bare electrostatic potential of the rod $\psi(r) = 2\xi \ln r$ [42]. This potential can be used to calculate the electrostatic energy (per number of monomers)

$$u_{elec} \approx f\xi \ln \frac{D}{R}, \tag{30}$$

where R is defined in Eq. (24) and ξ is related to the rod length L through Eq. (13). The residual entropic contribution of counterions may still be accounted for by assuming an ideal-gas entropy, s_{ci}, as in Eq. (25). The electrostatic free energy of the system is then written as $\mathcal{F}_{elec}/N \approx u_{elec} - s_{ci}$ which, for very large D/R_0, may be approximated by

$$\frac{\mathcal{F}_{elec}}{N} \approx f(\xi - 2) \ln \frac{D}{R}. \tag{31}$$

This expression is indeed a leading-order term and can be derived by expanding the PB free energy (8) in terms of R/D-powers (see Appendix B). Using Eqs. (31) and (24), the longitudinal electrostatic pressure can be calculated by differentiating $\mathcal{F}_{elec}$ with respect to $L = \xi_0 L_0/\xi$. Since the polyelectrolyte rod is again highly stretched in this limit, it is reasonable to approximate the elastic contribution by the same non-linear (logarithmic) expression, Eq. (26), as found in the strong-stretching limit. The equilibrium brush height is obtained by balancing these two contributions to the longitudinal pressure on the polyelectrolyte rod (*i.e.* using Eqs. (26) and (31)). The result (which has been calculated numerically) is shown in Figure 4 (dashed curve) for $f = 1$ and $\ell_B = 0.1b_0$, where we also show the results from minimization of the full free energy, Eq. (23) (solid curve a). The plot is made for $\rho_{\rm a}$ down to $10^{-6}b_0^{-2}$. For vanishingly small grafting densities $\rho_{\rm a} b_0^2 \to 0$, the entropic contributions become negligible compared with the bare electrostatic repulsion between monomers, and the equilibrium brush height behaves asymptotically as

$$\frac{L_*(\rho_{\rm a})}{L_0} \approx \frac{f \ln \rho_{\rm a} b_0^2}{f \ln \rho_{\rm a} b_0^2 - 2\xi_0^{-1}}. \tag{32}$$

This function is not shown in Figure 4, because it is valid for smaller grafting densities.

In the second scenario, *i.e.* when the optimal Manning parameter associated with the chains becomes larger than the threshold $\xi_* > \xi_c$, bare electrostatic interactions are partially screened as a result of the counterion-condensation process [39,40,41]. In fact, the PB electrostatic potential (up to some logarithmic corrections) reduces to the bare electrostatic potential of a rod with critical Manning parameter $\xi_M = 1$, *i.e.*, $\psi(r) = 2 \ln r$, when $D/R_0 \to \infty$ [38,42]. The electrostatic energy of the system for $D/R_0 \gg 1$ can be estimated using this potential, which yields

$$u_{elec} \approx \frac{f}{\xi} \ln \frac{D}{R}. \tag{33}$$

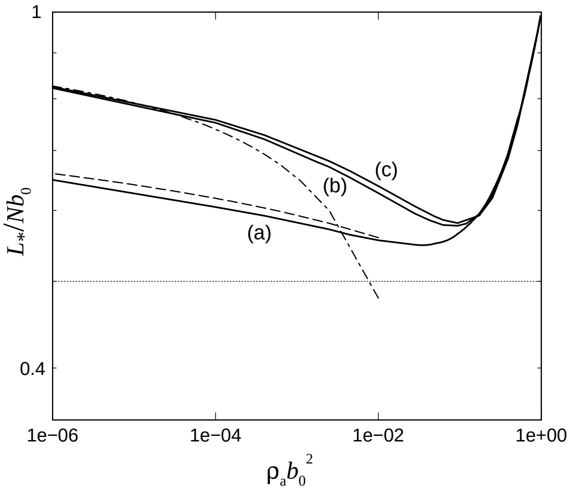

Fig. 4. Log-log plot of the rescaled optimal height of the brush as a function of grafting density. Solid curves show the results obtained from the minimization of the full free energy, Eq. (23), with $f = 1$, $q_c = q = 1$, and point-like counterions, for a) $\ell_B = 0.1b_0$ ($\xi_0 = 0.1$), b) $\ell_B = 0.7b_0$ ($\xi_0 = 0.7$) and c) $\ell_B = 1.2b_0$ ($\xi_0 = 1.2$). The dashed and dot-dashed curves show the corresponding asymptotic estimates at small grafting densities for the cases a) (using Eq. (31)) and c) (Eq. (35)) respectively. The dotted line shows the brush height in the absence of lateral effects for $f = 1$ (Eq. (36)).

To estimate entropic contributions in this case, we may adopt the counterion-condensation picture [39,40] that only a fraction of $1/\xi$ of counterions are unbound and may contribute to the entropic pressure. Thus, the corresponding ideal-gas entropy of counterions, s_{ci} in Eq. (25), may be corrected by such a factor and used, together with Eq. (33), to derive the leading term of the electrostatic free energy, $\mathcal{F}_{elec}/N \approx u_{elec} - s_{ci}$, as

$$\frac{\mathcal{F}_{elec}}{N} \approx -\frac{f}{\xi} \ln \frac{D}{R}. \tag{34}$$

The expression (34) is confirmed again by a limit expansion of the PB free energy (11)–see Appendix B. Calculating the longitudinal electrostatic pressure from Eq. (34) and balancing it with the non-linear stretching pressure from Eq. (26), one finds that

$$\frac{L_*(\rho_{\rm a})}{L_0} \approx 1 + \frac{2\xi_0}{f \ln \rho_{\rm a} b_0^2}. \tag{35}$$

The asymptotic expression, Eq. (35), is shown in Figure 4 (dot-dashed curve) along with the result from minimization of the full free energy, Eq. (23) (solid curve c) for a system with $f = 1$ and $\ell_B = 1.2b_0$ ($\xi_0 = 1.2$) for which the optimal Manning parameter, ξ_*, remains always above the threshold [38]. The above estimate, Eq. (35), represents the result obtained from the model for $\rho_{\rm a} b_0^2 < 10^{-4}$. At small grafting densities, the constant volume constraint becomes unimportant. We also note that within our model, similar behavior is obtained for the brush height for the whole range of Bjerrum lengths, see the result for $f = 1$ and $\ell_B = 0.7b_0$ ($\xi_0 = 0.7$) in Figure 4 (solid curve b).

The preceding discussion on the limiting behavior of the brush thickness demonstrates the important role of lateral electrostatic contributions to the total free energy that generate re-stretching of the chains at small grafting densities. Also we showed that the strength of these effects is controlled by the counterion-condensation process, which is systematically included in the PB equation used in Section 3.1 [33,41,42]. Both for weakly charged ($\xi_0 < 1$) and highly charged chains ($\xi_0 > 1$), lateral electrostatic contributions produce a repulsive longitudinal force acting on the chains, which logarithmically increases by decreasing the grafting density (Eqs. (31) and (34)). In particular, for highly charged chains, the force is independent of the brush height, *i.e.* $-\partial \mathcal{F}_{elec}/\partial L \sim \ln D/R$, and results from the electrostatic screening due to condensation of counterions (see Eqs. (34) and (13)). In any case, the increase of the brush height, which converges to the contour length, is logarithmically weak as the grafting density is lowered. We note that this behavior will not be obtained if lateral effects are neglected. In this case, the brush height remains independent of the grafting density,

$$\frac{L_*}{L_0} = \frac{f}{1+f}, \tag{36}$$

which is shown by a dotted line in Figure 4, and follows from balancing the entropic term, Eq. (25), and the non-linear elasticity, Eq. (26), where the volume constraint, Eq. (24), is also neglected

As already mentioned, our model describes the situation, in which counterions remain all inside the brush and distribute uniformly in the direction normal to the anchoring plane. In the range of parameters, when a considerable fraction of counterions leaves the brush (*e.g.* when chains are short or charge fraction is small), a different behavior will be obtained for the brush thickness as a result of the inhomogeneous distribution of counterions in the normal direction. In this case, if the concentration of counterions (and that of monomers) is assumed to be smeared out laterally, the brush height is obtained to decrease monotonically by lowering the grafting density as shown in Ref. [11]. Therefore, the behavior of the brush height in the presence of non-uniformities in both lateral and normal directions should be examined in an extended approach.

Finally, we remark that the non-monotonic behavior of the brush thickness is not influenced by the elasticity model and qualitatively similar features are obtained when a Gaussian chain elasticity is used [43].

4 Comparison to molecular dynamics simulations

Computer simulations provide an excellent mean to study polymer systems. Extensive molecular dynamics simulations have been performed recently on polyelectrolyte brushes at various grafting densities and charge fractions, both at strong [13,14,15] and intermediate [16] electrostatic couplings.

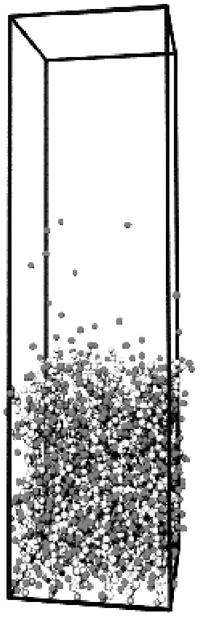

Fig. 5. A snapshot of the simulated polyelectrolyte brush with 36 fully charged chains of $N = 30$ monomers (in light gray) at grafting density of $\rho_{\mathrm{a}} = 0.12\sigma^{-2}$. The Bjerrum length is $\ell_B = \sigma$. Counterions are shown by dark gray spheres. The box height perpendicular to the anchoring plane has been reduced for the sake of representation.

In these simulations, a freely-jointed bead-chain model is adopted where the monomers are connected by non-linear springs with the so-called FENE (finite extensible non-linear elastic) potential, and end-grafted onto a rigid surface. The counterions are explicitly modeled as charged particles and no additional electrolyte is added. The simulation box is periodic in lateral directions and finite in the z-direction normal to the anchoring surface at $z = 0$. We use the techniques introduced in Refs. [44,45] to account for the long-range nature of the Coulombic interactions in a laterally periodic system. The short-range repulsion between particles separated by distance r is modeled by a shifted Lennard-Jones (LJ) potential $u(r) = 4\epsilon_{LJ}\{(\sigma/r)^{12} - (\sigma/r)^6 + 1/4\}$ for $r/\sigma \leq 2^{1/6}$ and $u(r) = 0$ otherwise, with Lennard-Jones diameter of σ being equal for both monomers and counterions. The counterions and charged monomers are univalent ($q_c = q = 1$). For the simulations reported below, we choose moderate values for the Bjerrum length, *i.e.* $\ell_B = \sigma$ and $\ell_B \approx 2\sigma$, which correspond to electrostatically-intermediate-coupling situation. With this choice of parameters, the average bond length (which is the result of the interplay between LJ repulsion and the FENE bond potential) is almost unaffected by the electrostatic repulsions and is $b_0 = 0.98\sigma$.

Figure 5 shows a snapshot from the simulation of a brush with 36 chains of 30 monomers, which is fully charged and has a large grafting density of $\rho_{\mathrm{a}} = 0.12\sigma^{-2}$. In this figure, the connectivity of the chains are preserved, so that the chains may appear to extend beyond the sim-

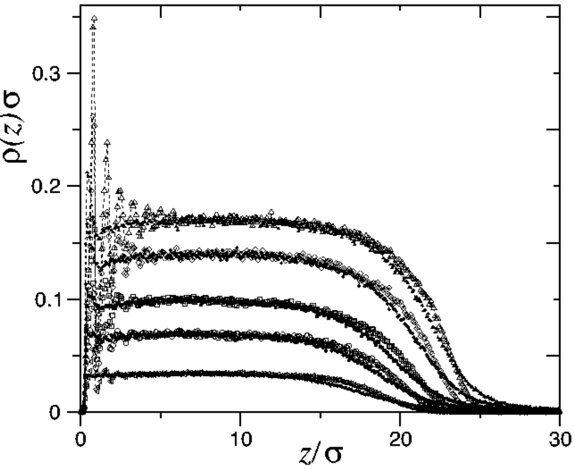

Fig. 6. Density profiles of monomers $\rho_m(z)$ (open symbols) and counterions $\rho_{ci}(z)$ (filled symbols) as a function of the distance from the anchoring surface. Shown are profiles for fully charged brushes of 36 chains of $N = 30$ monomers at $\ell_B = \sigma$ and grafting densities (from bottom to top) $\rho_a\sigma^2 = 0.020$ (triangle-lefts), 0.042 (circles), 0.063 (squares), 0.094 (diamonds), and 0.12 (triangle-ups).

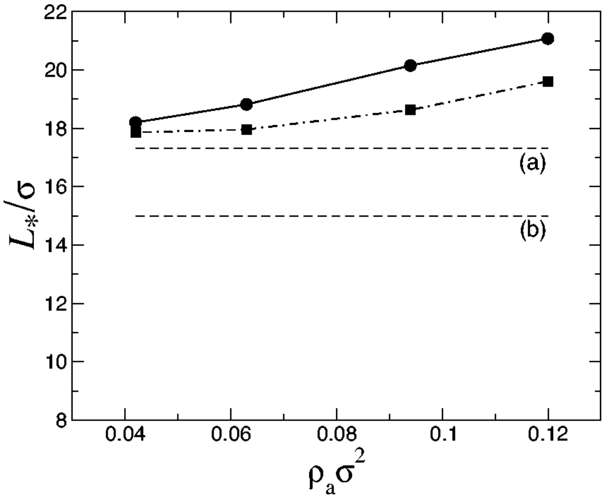

Fig. 7. Brush height as a function of grafting density for polyelectrolyte chains of $N = 30$ monomers (contour length $L_0 = 30\sigma$) with charge fraction of $f = 1$. Circles show the simulation data and squares are the predictions of the present mean-field model. The dotted lines (a) and (b) show the scaling predictions, Eqs. (37) and (36), with Gaussian and non-linear elasticity respectively. Here Bjerrum length is $\ell_B = \sigma$ and charged particles are univalent.

ulation box. (The simulation image has been produced using the VMD software package [46].) Simulated density profile of monomers and counterions of the system in normal direction are shown in Figure 6 for the fully charged brush at several grafting densities. As seen, both monomers and counterions follow very similar nearly-step-like profiles with uniform amplitude inside the brush, which increases with grafting density (the monomers show a short-range ordering close to the anchoring plane, which is not relevant in the present study). These figures show that the counterions are mostly confined in the brush layer and that the electroneutrality condition is satisfied locally [16]. One may observe (more clearly from simulated brush heights in Figures 7 and 8) that the polyelectrolyte chains are stretched up to about 60% of their contour length, and thus their elastic behavior is far beyond the linear regime. Therefore, within the chosen range of parameters, the simulated brush is in the strong-charging and strong-stretching limits and as we will show, it exhibits the non-linear osmotic brush regime.

The average height of endpoints of the chains is one of the quantities which can be directly measured in the simulations. We compare the predictions of our theoretical model for the brush height with the average height of the endpoints from our simulations in Figures 7 and 8 for charge fractions $f = 1$ (with $\ell_B = \sigma$) and $f = 1/3$ (with $\ell_B \approx 2\sigma$) respectively. To obtain theoretical data from the model, we have taken into account the finite size of the counterions using $r_c = b_0/2$; moreover, we take $b_0 = \sigma$ while comparing these data with the simulation results.

As seen from the Figures, the simulated brush height (circles) varies slowly with the grafting density, contrary to the predictions of scaling theories. According to the scaling studies [3,4,7], the osmotic brush thickness is obtained as

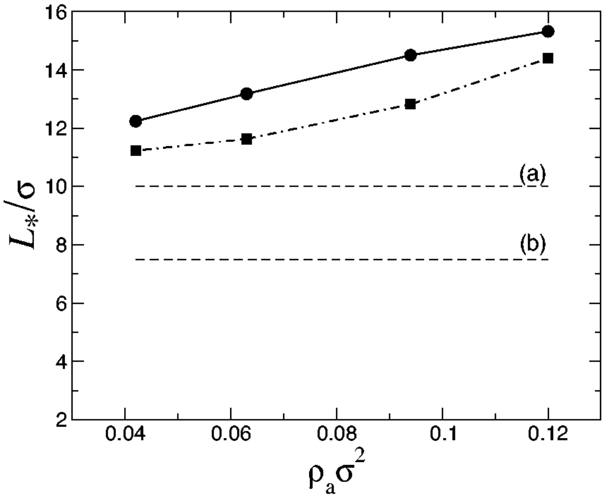

Fig. 8. Same as Figure 7 but for $f = 1/3$ and Bjerrum length $\ell_B \approx 2\sigma$.

$$L_{OsB} = \frac{1}{\sqrt{3}} N f^{1/2} b_0, \tag{37}$$

which is independent of the grafting density (shown by dotted line (a) in the Figures). This relation is based on a balance between the osmotic pressure of an ideal gas of counterions inside the brush $\pi_{os} = N f \rho_a / L$, and the elasticity of Gaussian chains, $\pi_{elas} = 3\rho_a L / N b_0^2$. If we adopt the non-linear elasticity for large stretching, Eq. (26), the brush height is given by Eq. (36), when lateral effects are neglected. The result is also independent of the grafting density and shown by dotted line (b) in Figures 7 and 8. The present model considers corrections to the scaling theory by accounting for lateral electrostatic and coupling effects. The theoretical predictions (squares) appear to be in reasonable agreement with the simulation results. As shown in Ref. [34] by comparing different cell models for the brush, the deviations from the simulation data are in fact of the oder of the systematic error of the employed cylindrical cell model (Section 2). In other words, choosing a different cell volume or a different rod model for the polymer chain leads to differences in theoretical predictions that are of the same order as the deviations from the simulation data in Figures 7 and 8. Yet some of the differences may be in general due to excluded-volume effects that have been treated in a simplified way in our study. In particular, we have neglected the excluded-volume repulsion between counterions; a rough estimate of these effects, however, shows that such volume effects are almost one order of magnitude smaller than the osmotic pressure of counterions (see the Discussion).

Another effect which may play a role in the simulated systems is lateral wiggling of the polyelectrolyte chains. In fact, the volume constraint, that has been used in our model, can account for some of these effects in a very simple way, since the effective chain radius increases for decreasing brush height. However, conformational changes of the chains may affect the validity of the cell model that was employed for calculating the electrostatic contributions to the free energy. From lateral monomer density profile obtained within the simulations [47], we conclude that wandering of chains is well-confined to a cylindrical region, the size of which is smaller than the "cell radius". The cell radius is close to the decay range of the lateral monomer density profile only for large grafting densities, thus in this regime, lateral wiggling of the chains might be responsible for some of the deviations between the theoretical predictions and the simulation data.

5 Conclusion and Discussion

We have studied strongly charged polyelectrolyte brushes in the non-linear osmotic regime. In order to bring out the features of the non-linear osmotic brush regime more clearly, we chose a moderate Bjerrum length of the order of the monomer size in our simulations. Nonetheless, the present theory is obtained for the whole range of Bjerrum lengths, and similar features are obtained at large, more realistic values of the Bjerrum length (see Section 3.3).

In the simulations [16], we have observed that the brush height varies slowly with the grafting density of the brush. In this situation, polyelectrolyte chains are strongly stretched and counterions are mostly confined within the brush layer. In the direction normal to the anchoring plane, counterions produce an almost step-like density profile, while in lateral directions, an inhomogeneous distribution is observed around polyelectrolyte chains at moderate grafting densities [14,15,16].

We have investigated this system using a theoretical model, in which we consider a number of corrections to the standard scaling theories. Firstly, the electrostatic free energy of the system is calculated within the non-linear Poisson-Boltzmann theory, which includes lateral electrostatic effects. On the other hand, the elastic free energy of the chains is calculated using a freely-jointed-chain model providing a non-linear elasticity in the strong-stretching limit, which accounts for the finite extensibility of the brush chains. We have taken into account also the back influence of the conformational changes of the chains on the osmotic pressure of counterions. Such a coupling between longitudinal and lateral degrees of freedom is modeled in a simple way by assuming a constant effective volume for the chains. The results of our model display a non-monotonic behavior for the brush height as a function of the grafting density. In particular, at moderate grafting densities, we find that the brush height weakly increases with grafting density, which arises as a result of the interplay between lateral electrostatics and the coupling (volume constraint) effect. This behavior agrees with the simulation data within the systematic error of our model; the deviations may originate mainly from non-uniform boundary conditions in the simulations. Predictions of our model also agree with recent experiments on osmotic brushes on a semi-quantitative level as discussed in Refs. [26,27].

As already discussed, the behavior of the brush height at very large grafting densities (closely-packed brush) is dominated by the volume constraint used in our model. The characteristic of this regime is the linear increase of the brush height with grafting density (see Eq. (28)). In this regime, excluded-volume effects become relevant and should be considered explicitly in the balance equations. While, in our study, volume interactions are only effectively modeled. Nonetheless, at lower grafting densities (*e.g.* at about $\rho_{\mathrm{a}} b_0^2 \sim 0.1$ as investigated in the simulations), lateral electrostatic effects involved in the PB free energy become increasingly important and lead to a weaker increase of the brush height with grafting density (see Figure 3).

For large grafting densities, possible contribution of the excluded-volume repulsions between counterions may be estimated as follows. Effectively, the second-virial contribution from counterions to the total free energy (per unit cell and in units of $k_B T$) may be written as

$$\frac{\mathcal{F}_{v2}}{N} = \frac{1}{2N} v_2\, \overline{\rho}_{ci}^2 V_{cell} = \frac{1}{2} v_2 \frac{N f^2}{\pi(D^2 - R^2)L}, \tag{38}$$

where $v_2 > 0$ is the effective virial coefficient (for good solvent condition), and $\overline{\rho}_{ci}$ is the average density of counterions in a unit cell of volume $V_{cell} = \pi(D^2 - R^2)L$. The longitudinal pressure coming from the excluded-volume repulsions between counterions, π_{v2}^{Long}, is calculated by differentiating Eq. (38) with respect to L, the brush height. The produced pressure is then compared with the longitudinal osmotic pressure of counterions obtained from Eq. (25), that is $\pi_{os}^{Long} \sim f/L$. We find

$$\frac{\pi_{v2}^{Long}}{\pi_{os}^{Long}} \sim \frac{v_2/2\pi b_0^3}{L/N f b_0} \left(\frac{4\rho_{\mathrm{a}} b_0^2}{1 - 4\rho_{\mathrm{a}} b_0^2} \right), \tag{39}$$

where we have also considered the closest approach distance between counterions and monomers as discussed in the text (here we have taken univalent particles for simplification). Now, for largest grafting densities used in the simulations, *e.g.* $\rho_a b_0^2 \sim 0.1$, and for fully charged chains $f = 1$ (where $L/L_0 \sim 2/3$), it follows that $\pi_{v2}^{Long}/\pi_{os}^{Long} \sim (1/10) v_2/v_2^{HC}$, where $v_2^{HC} = \pi b_0^3/6$ is the hard-core second virial coefficient. This ratio is even smaller for smaller charge fractions and grafting densities, and roughly yields the largest estimate based on the simulation data. Clearly, if we assume that $v_2 \sim v_2^{HC}$, the excluded-volume pressure of counterions, which is neglected in our model, is found to be almost one order of magnitude smaller than their osmotic pressure.

At small grafting densities, our model predicts a weak re-stretching of the chains by lowering the grafting density, which is produced by lateral electrostatic contributions and is controlled by lateral rearrangement of counterions (counterion-condensation process) around the chains (Section 3.3). These results are valid only if the optimal height of the brush is much larger than the distance between neighboring grafted chains. (In particular, the counterion condensation occurs in the presence of long chains, when end effects are negligible.) This situation may be achieved by taking polyelectrolyte chains with sufficiently large contour length and at large charge fractions. Otherwise, the cylindrical symmetry, assumed in the calculation of the electrostatic free energy, and also the osmotic conditions are no longer retained. We may estimate the regime of validity of our results as follows. At small grafting densities, a large fraction of counterions tends to leave the brush and consequently, the system is pushed away from the osmotic regime: for large charge fractions, it will enter the Pincus brush regime, where uncompensated electrostatic repulsion between monomers balances the elastic stretching, and for small charge fractions of the chains, mushroom conformations, that are entropically favorable, are formed by shrinkage of the chains onto the anchoring plane. The crossover from osmotic to Pincus brush regime can be identified by introducing the average height of the counterion layer over the anchoring plane. The thickness of the counterion layer is in fact characterized by the effective Gouy-Chapman length of the plane, that is $\lambda_{GC} = 1/2\pi \ell_B N f \rho_a$ (we restrict our discussion to the case with univalent particles). In the osmotic brush regime, where the surface charge density $N f \rho_a$ is large, one has $\lambda_{GC} \leq L$, whereas in Pincus brush regime with small surface charge density $\lambda_{GC} \gg L$. (In the simulations, we have $\lambda_{GC}/L \sim 10^{-3}$ for $f \sim 1$ and $\rho_a b_0^2 \sim 0.1$.) To retain counterions inside the brush, one needs to take polyelectrolyte chains with number of monomers N larger than a certain threshold number N_*. To estimate N_*, one can use scaling arguments that yield Pincus brush height as [3]

$$L_{PB} \sim N^3 \ell_B f^2 \rho_a b_0^2. \tag{40}$$

Now, given the scaling relations for the osmotic and Pincus brush regimes, Eqs. (37) and (40) respectively, one can find the boundary relation between these two regimes as $N^2 f^{3/2} \ell_B \rho_a b_0 \sim 1$ [9]. The threshold number of monomers N_* follows from this relation, *i.e.*,

$$N_* = f^{-3/4} (\rho_a b_0^2)^{-1/2} (\frac{b_0}{\ell_B})^{1/2}. \tag{41}$$

One notes that for $f \sim 1$ and $\ell_B \sim b_0$ this corresponds to the overlapping threshold for neighboring chains, that is when $\rho_a L_0^2 \sim 1$ with $L_0 = N b_0$ as the contour length of the chains. To give a numerical estimate of N_*, we use the simulation parameter $\ell_B = b_0$ for fully charged chains ($f = 1$): at grafting densities as small as $\rho_a b_0^2 \sim 10^{-6}$, Eq. (41) gives $N_* \sim 10^3$, while for $\rho_a b_0^2 \sim 10^{-2}$ we would have $N_* \approx 10$. Note that the latter case coincides with the minimum grafting density used in the simulations (see Section 4), where polyelectrolyte chains bear $N = 30$ monomers.

Now, to prevent formation of mushrooms at small grafting densities and *small charge fractions*, one may take longer chains with $N > N_{**} = (\rho_a b_0^2)^{-1}$, which is a more stringent condition on N, *i.e.* $N_{**} > N_*$. This corresponds to the condition that the Gaussian size of the polyelectrolyte chains, $N^{1/2} b_0$, be larger than the distance between neighboring chains $\rho_a^{-1/2}$. (Note that we have assumed a Gaussian polymer, thus our estimate gives an upper bound for N_{**}.) At small grafting density of $\rho_a b_0^2 \sim 10^{-6}$, one has $N_{**} \sim 10^6$, a quite large value, and for $\rho_a b_0^2 \sim 10^{-2}$, we obtain $N_{**} \sim 100$. We conclude that the regime, where the brush height has been predicted to increase with decreasing the grafting density is observable in experiments and simulations by choosing long enough chains.

In this paper the system is studied within a mean-field approximation, which is valid only if electrostatic correlations are negligible. Such effects become important at strong electrostatic couplings [48], *i.e.* at large Bjerrum lengths and charge valencies, and can produce significant attractive pressure on the chains. In such conditions, a scaling theory has been developed which predicts a collapsed brush regime observed also in simulation [13]. At moderate Bjerrum length and for univalent particles as chosen in our simulations, correlation effects are not yet important, and as we showed, the predictions of the present mean-field theory are very close to the simulation results.

An interesting problem is to extend the present results to include the variation of the counterionic density profile in the direction normal to the anchoring plane, which may be caused by the diffusion of counterions outside the brush at low grafting densities or at small charge fractions. The self-consistent field analysis of Zhulina and Borisov [11] reveals that if these effects are accounted for using the non-linear PB equation, the brush height monotonically decreases by lowering the grafting density provided that the concentration of counterions (and that of monomers) is assumed to be smeared out laterally. Our results show a re-increase of the brush height by lowering the grafting density, when the counterion profile is assumed to be uniform in normal direction, and allowed to admit a laterally inhomogeneous form according to the non-linear PB equation. An extended approach should, therefore, examine the interplay between these two mechanisms.

Finally, we remark that similar calculations can be done for slightly different models [34], *e.g.* one may consider a volume charge distribution for polyelectrolyte chains. Clearly, the Coulomb self-energy of the polymer would be larger in this case and a larger brush height is predicted as compared with the studied model.

We acknowledge discussions with O. Borisov and N.A. Kumar. We also thank H. Ahrens, C.A. Helm, and G. Romet-Lemonne, J. Daillant, and P. Guenoun for communication about their recent experimental data. A.N. acknowledges financial support from the DFG Schwerpunkt Polyelektrolytes with defined architecture and the DFG German-French Network. C.S. gratefully acknowledges grants for computer time at the John von Neumann-Institut for Computing (NIC) Jülich and the Konrad Zuse Zentrum für Informationstechnik Berlin (ZIB).

A The free energy of a freely-jointed chain

We calculate the free energy of a freely-jointed chain consisting of N links (monomers), each of fixed length b_0 and able to point in any direction independently of each other. It is convenient to perform the calculation in an isobaric ensemble, in which the chain is considered to be stretched by applying a constant force F (in units of k_BT). Since the monomers are assumed as rigid links, the configuration space of the chain is spanned by a set of angles $\{\theta_i, \phi_i\}$ specifying orientations of the monomers labeled by $i = 1, \ldots, N$ (a standard spherical frame of coordinates is chosen with z-axis pointing in the same direction as the force). The partition function of such a polymer chain can be written as

$$\mathcal{Z}_F = \left[\int_0^{2\pi} \frac{d\phi}{2\pi} \int_0^{\pi} \frac{d\theta}{2} \sin\theta \, e^{b_0 F \cos\theta}\right]^N. \tag{42}$$

Integrating Eq. (42) we find

$$\mathcal{Z}_F = \left[\frac{e^{b_0 F} - e^{-b_0 F}}{2 b_0 F}\right]^N. \tag{43}$$

Now, the extension (end-to-end distance) of the chain, L, is calculated from $L = \partial \ln \mathcal{Z}_F / \partial F$ as

$$\frac{L}{b_0 N} = \coth b_0 F - \frac{1}{b_0 F}. \tag{44}$$

Using Legendre transformation we can calculate the isochoric free energy of the system (in units of k_BT), $\mathcal{F}^{FJC} = -\ln \mathcal{Z}_F + LF$, hence

$$\frac{\mathcal{F}^{FJC}}{N} = -\ln \frac{\sinh b_0 F}{b_0 F} + b_0 F \coth b_0 F - 1, \tag{45}$$

which was used together with Eq. (44) in Section 3.2.

In the weak-stretching or Gaussian-chain limit $b_0 F \ll 1$, the end-to-end distance is obtained by a proper expansion of Eq. (44) as $L \approx N b_0^2 F/3$, which is then used to get the free energy $\mathcal{F}^{FJC}/N \approx 3L^2/2(Nb_0)^2$. In the strong-stretching limit $b_0 F \gg 1$, a non-linear force-extension relation is reached from Eq. (44), that is $L/b_0 N \approx 1 - 1/b_0 F$. Using this, we find the elastic free energy $\mathcal{F}^{FJC}/N \approx -\ln(1 - L/N b_0) + const.$

B Asymptotic expansions of the PB free energy

Here, we briefly discuss the asymptotic expansions of the PB free energy both in the limit of small and large grafting densities. For simplicity, we assume $q_c = q$.

B.1 Small grafting densities ($D/R \gg 1$):

In this case, there are different limit expansions for the PB free energy depending on whether the Manning parameter is smaller or larger than ξ_c. Note that in this limit, the threshold Manning parameter itself tends to one, *i.e.* $\xi_c \to 1$ (see Eq. (18), also Ref. [31]).

B.1.1 Case with $\xi \le \xi_c$.

Inspecting Eq. (7), one can find that in the limit of $D/R \to \infty$, the solution for β tends asymptotically to $\beta = (\xi - 1)$. Hence for $D/R \gg 1$, we can propose the following form for β,

$$\beta^2 \approx (\xi - 1)^2 (1 - x), \tag{46}$$

where x is a small function of ξ and D/R, and may be determined as follows. Rearranging Eq. (7), we can find a more convenient equation for the forthcoming limit expansions,

$$\beta \ln \frac{D}{R} = \frac{1}{2} \ln \frac{1-\beta}{1+\beta} - \frac{1}{2} \ln \frac{(\xi - 1) + \beta}{(\xi - 1) - \beta}. \tag{47}$$

Now using Eq. (46) into Eq. (47) and expanding for small x, we have

$$x \approx \frac{4\xi}{2-\xi} \left(\frac{D}{R}\right)^{2(\xi-1)}. \tag{48}$$

Similar limit expansions can be performed for the potential field, Eq. (6), and the PB free energy, Eq. (8), with x given by Eq. (48), which lead to

$$\psi(r) \approx 2\xi \ln \frac{r}{R}, \tag{49}$$

(where we have assumed $\psi(R) = 0$), and

$$\frac{\mathcal{F}^{PB}}{N} \approx f(\xi - 2) \ln \frac{D}{R}, \tag{50}$$

as estimated in Eq. (31) in the text. Clearly, both bare electrostatic repulsions of the charged rod and entropy of mobile counterions contribute in Eq. (50) respectively as $f\xi \ln D/R$ and $-2f \ln D/R$. However, in the limit of very large D/R, the longitudinal entropic pressure of counterions becomes vanishingly small relative to the longitudinal bare electrostatic pressure. This can be seen from Eq. (50), noting that the longitudinal pressure is obtained by differentiation of the corresponding term in the free energy with respect to the cell volume $\pi D^2 L$ at fixed cell radius D. Formally, the longitudinal osmotic pressure, π_{os}^{Long}, will be $\pi_{os}^{Long} = -\partial \mathcal{F}_{elec}/\pi D^2 \partial L$, where L is related to ξ via Eq. (13) and $\mathcal{F}_{elec}$ is given by Eq. (50).

In contrast, both bare electrostatic repulsions and entropic effects produce lateral pressures of the same leading order. (The lateral pressure is obtained by differentiation of the corresponding term in the free energy with respect to $\pi D^2 L$ at fixed rod length L.) The latter result is known as Manning limiting law for osmotic coefficient of dilute solutions of weakly charged polyelectrolytes [40]. This limiting law follows directly from Eq. (50) as we explain now.

For rod-like polyelectrolytes with $\xi \leq \xi_c$, the Manning limiting law states that the osmotic coefficient, ν, tends to a finite value as the solution becomes highly diluted,

$$\lim_{D/R\to\infty} \nu = (1 - \frac{\xi}{2}). \tag{51}$$

The osmotic coefficient here is defined as the ratio of the lateral osmotic pressure acting on the cell boundary,

$$\pi_{os}^{Lat}(D) = -\frac{\partial \mathcal{F}_{elec}}{2\pi D L \partial D} \tag{52}$$

to the lateral osmotic pressure of an ideal gas of particles, P_{id}, filling the cell under similar conditions, *i.e.*

$$\nu = \frac{\pi_{os}^{Lat}}{P_{id}}. \tag{53}$$

Now, given the ideal-gas pressure $P_{id} = N_c/\pi L(D^2 - R^2)$ and the (PB) electrostatic free energy of Eq. (50), one can easily recover the limiting law, Eq. (51), using Eqs. (52) and (53).

B.1.2 Case with $\xi \geq \xi_c$.

In this case, it follows from Eq. (10) that β tends to zero (as $(\ln D/R)^{-1}$) when $D/R \to \infty$. Using this, one can observe that the potential field of Eq. (9) reduces to

$$\psi(r) \approx 2\ln\frac{r}{R} + 2\ln[1 + (\xi - 1)\ln\frac{r}{R}], \tag{54}$$

and the PB free energy, Eq. (11), to

$$\frac{\mathcal{F}^{PB}}{N} \approx -\frac{f}{\xi}\ln\frac{D}{R}, \tag{55}$$

as estimated heuristically in Eq. (34) in the text. Clearly in this case when $\xi > \xi_c$, unlike the case with $\xi < \xi_c$, electrostatic repulsions and entropic effects have contributions of the same order of magnitude in the total longitudinal pressure which acts on the rod. This result may be understood in terms of the counterion condensation model [40] as explained in Section 3.3.

The Manning limiting law for the (lateral) osmotic coefficient is now obtained (from Eqs. (52), (53) and (55)) as

$$\lim_{D/R\to\infty} \nu = \frac{1}{2\xi}, \tag{56}$$

where $\xi \geq \xi_c$.

In our model where R is not fixed but depends on ξ (see Eq. (15)), the preceding discussions hold when $D \gg r_c + R_0$.

B.2 Large grafting densities ($D/R \approx 1$):

In a cell model with fixed R, the threshold Manning parameter ξ_c tends to zero as $D/R \to 1$ [31]. Therefore, for finite values of the Manning parameter ξ, we have to use Eqs. (10) and (11) for $\xi \geq \xi_c$.

Starting from Eq. (10), we can find an approximate expression for β in the limit of $D/R \to 1$. Defining $\delta = D/R - 1$ and expanding Eq. (10) for small δ, we obtain

$$\beta^2 \approx \xi(\frac{1}{\delta} + \mathcal{O}(\delta^0)) - 1. \tag{57}$$

Now replacing β^2 in Eq. (11) and expanding in terms of δ, we have (up to an additive constant independent of δ)

$$\frac{\mathcal{F}^{PB}}{N} \approx -f\ln\delta + \mathcal{O}(\delta). \tag{58}$$

This is the entropic free energy of an ideal gas of particles (Eq. (25)) up to the leading order, and shows that in this limit, the main contribution to the PB free energy comes from the entropy of counterions.

In our model with the constant volume constraint, this limit (namely $D \to r_c + R_0$) has to be handled with care. In fact, the upper limit on ξ, that is ξ_u, tends to the lower limit ξ_0, and so does the optimal Manning parameter. The threshold ξ_c becomes smaller than ξ_0, therefore, the system indeed satisfies $\xi > \xi_c$ condition [38], so that the above discussion remains valid.

References

1. S.J. Miklavic, S. Marcelja, J. Phys. Chem. **92**, 6718 (1988).
2. S. Misra, S. Varanasi, P.P. Varanasi, Macromolecules **22**, 4173 (1989).
3. P. Pincus, Macromolecules **24**, 2912 (1991).
4. O.V. Borisov, T.M. Birstein, E.B. Zhulina, J. Phys. II (Paris) **1**, 521 (1991).
5. R.S. Ross, P. Pincus, Macromolecules **25**, 2177 (1992).
6. E.B. Zhulina, T.M. Birstein O.V. Borisov, J. Phys. II (Paris) **2**, 63 (1992).
7. J. Wittmer, J.-F. Joanny, Macromolecules **26**, 2691 (1993).
8. R. Israëls, F.A.M. Leermakers, G.J. Fleer, E.B. Zhulina, Macromolecules **27**, 3249 (1994).
9. O.V. Borisov, E.B. Zhulina, T.M. Birstein, Macromolecules **27**, 4795 (1994).
10. V.A. Pryamitsyn, F.A.M. Leermakers, G.J. Fleer, E.B. Zhulina, Macromolecules **29**, 8260 (1996).

11. E.B. Zhulina, O.V. Borisov, J. Chem. Phys. **107**, 5952 (1997).
12. V.M. Amoskov, V.A. Pryamitsyn, Polymer Science USSR **37**, 1198 (1995).
13. F.S. Csajka, R.R. Netz, C. Seidel, J.-F. Joanny, Eur. Phys. J. E **4**, 505 (2001).
14. F.S. Csajka, C.C. van der Linden, C. Seidel, Macromol. Symp. **146**, 243 (1999).
15. F.S. Csajka, C. Seidel, Macromolecules **33**, 2728 (2000); Macromolecules **38**, 2022 (2005).
16. C. Seidel, Macromolecules **36**, 2536 (2003); Macromolecules **38**, 2540 (2005).
17. Y. Mir, P. Auroy, L. Auvray, Phys. Rev. Lett. **75**, 2863 (1995).
18. P. Guenoun, A. Schlachli, D. Sentenac, J.M. Mays, J.J. Benattar, Phys. Rev. Lett. **74**, 3628 (1995).
19. H. Ahrens, S. Förster, C.A. Helm, Macromolecules **30**, 8447 (1997).
20. H. Ahrens, S. Förster, C.A. Helm, Phys. Rev. Lett. **81**, 4172 (1998).
21. F. Muller, M. Delsanti, L. Auvray, J. Yang, Y.J. Chen, J.W. Mays, B. Demé, M. Tirrell, P. Guenoun, Eur. Phys. J. E **3**, 45 (2000).
22. F. Muller, P. Fontaine, M. Delsanti, L. Belloni, J. Yang, Y.J. Chen, J.W. Mays, P. Lesieur, M. Tirrell, P. Guenoun, Eur. Phys. J. E **6**, 109 (2001).
23. P. Guenoun, F. Muller, M. Delsanti, L. Auvray, Y.J. Chen, J.W. Mays, M. Tirrell, Phys. Rev. Lett. **81**, 3872 (1998).
24. M. Balastre, F. Li, P. Schorr, J. Yang, J.W. Mays, M.V. Tirrell, Macromolecules **35**, 9480 (2002).
25. S. Hayashi, T. Abe, N. Higashi, M. Niwa, K. Kurihara, Langmuir **18**, 3932 (2002).
26. H. Ahrens, S. Förster, C.A. Helm, N.A. Kumar, A. Naji, R.R. Netz, C. Seidel, J. Phys. Chem. B **108**, 16870 (2004).
27. G. Romet-Lemonne, J. Daillant, P. Guenoun, J. Yang, J.W. Mays, Phys. Rev. Lett. **93**, 148301 (2004).
28. D.H. Napper, *Polymeric Stabilization of Colloidal Dispersions* (Academic Press, New York, 1983).
29. Y.S. Park, Y. Ito, Y. Imanishi, Chem. Mater. **9**, 2755 (1997).
30. T. Alfrey, P.W. Berg, H. Morawetz, J. Polymer Sci. **7**, 543 (1951).
31. R.M. Fuoss, A. Katchalsky, S. Lifson, Proc. Natl. Acad. Sci. USA **37**, 579 (1951).
32. A. Katchalsky, Pure Appl. Chem. **26**, 327 (1971).
33. C. Holm, P. Kékicheff, R. Podgornik (Editors), *Electrostatic Effects in Soft Matter and Biophysics* (Kluwer Academic Publishers, Dordrecht, 2001).
34. A. Naji, R.R. Netz, C. Seidel, Eur. Phys. J. E **12**, 223 (2003).
35. S. Lifson, A. Katchalsky, J. Polymer Sci. **13**, 43 (1954).
36. R.R. Netz, H. Orland, Eur. Phys. J. E **1**, 67 (2000).
37. The electroneutrality condition entails that the canonical free energy, Eq. (1), be invariant under the gauge transformation $\psi \to \psi + \psi_0$. As a consequence, the PB free energy (see Eqs. (8) and (11)) is independent of κ^2.
38. It is easy to check that the threshold Manning parameter, ξ_c, tends to the so-called Manning critical value $\xi_M = 1$ (the onset of counterion condensation [39,40]), when $D \to \infty$, or R_0 and $r_c \to 0$. In our model, the threshold Manning parameter ξ_c may be smaller or larger than ξ_0, but it never exceeds ξ_u defined in Eq. (17), *i.e.* $\xi_c < \xi_u$. Also it never becomes larger than one as it follows easily from Eq. (18). Therefore, in a system with $\xi_0 > 1$, we will always have the above-threshold condition $\xi \geq \xi_0 > \xi_c$ implied by Eq. (16). Similar situation occurs when $D \to R_0 + r_c$, since in this case we have $\xi_u \to \xi_0$, and hence, again ξ_c lies below ξ_0.
39. F. Oosawa, *Polyelectrolytes* (Marcel Dekker, New York 1971).
40. G.S. Manning, J. Chem. Phys. **51**, 924 (1969).
41. M. Le Bret, B.H. Zimm, Biopolymers **23**, 287 (1984).
42. R.R. Netz, J.-F. Joanny, Macromolecules **31**, 5123 (1998).
43. Replacing the FJC elasticity with the Gaussian chain elasticity given in Eq. (21), the brush height is found to increase logarithmically by decreasing the grafting density in the low-grafting-density regime. For instance, we obtain $L_*/L_0 \sim -\ln \rho_{\mathrm{a}} b_0^2$ for highly charged chains. Note that the elasticity model affects the magnitude of the stretching of the chains and also the particular dependence of the brush height on the grafting density (although it can not produce a grafting-density dependence by itself [12]). For chains of finite length, the correct limiting dependence is obtained if we take into account the finite extensibility of the chains, which is mimicked by the FJC model.
44. R. Strebel, R. Sperb, Mol. Simul. **27**, 61 (2001).
45. A. Arnold, C. Holm, Comput. Phys. Commun. **148**, 327 (2002).
46. W. Humphrey, A. Dalke, K. Schulten, J. Molec. Graphics **14**, 33 (1996).
47. C. Seidel, unpublished.
48. R.R. Netz, Eur. J. Phys. E **5**, 557 (2001).